Light Metals 2015
Edited by: Margaret Hyland
TMS (The Minerals, Metals & Materials Society), 2015

THERMAL STRESS PREDICTION IN AA5182 RECTANGULAR INGOTS

Yunbo Wang[1], Matthew John M. Krane[1], Kevin P. Trumble[1]
[1]Purdue Center for Metal Casting Research, School of Materials Engineering, Purdue University,
701 Northwestern Avenue, Neil Armstrong Hall of Engineering,
West Lafayette, IN 47907, USA

Keywords: Aluminum, DC Casting, Simulation, Slabs

Abstract

In DC casting of aluminum alloys, thermal strains can cause cracks during and after solidification and rejection of the ingot. Previous numerical models have simulated strain and stress in rounds, but less attention has been paid to slabs. To study residual stresses as a function of rectangular ingot aspect ratio and absolute ingot size, a 3D finite element model is used with simplified dynamic thermal boundary conditions. In industrial practice, a wiper is sometimes placed below the mold to isolate the lower part of ingot from cooling water, and that effect is also simulated. Stresses throughout the process start-up are predicted; the surface is first under tension, and later in compression, while the center has the opposite history. Results indicate decreasing stress magnitudes with the addition of a wiper. Also, placing the wiper closer to the mold will further reduce the residual tension in ingot center, but, if the wiper is too close, the ingot surface temperature will rebound and the surface may begin to remelt. A height limit of wiper position is determined to prevent the surface remelting. Larger ingots and slabs with larger aspect ratios are found out to have a higher overall tension level.

Introduction

Direct chill (DC) casting is the most common technology for production of aluminum alloy ingots. In this process, the liquid alloy first is cooled while moving through a mold to form a solid shell, and then exposed to direct contact with chilling water as it moves out of the mold. Due to the high and non-uniform heat extraction rate during DC casting, thermal strains accumulate and give rise to the development of residual stress. Tensile residual stress may result in crack formation during or after solidification, and cause hazards in the subsequent sawing process.

The early models on DC casting only dealt with the heat transfer of the solidification process [1, 2]. Beginning in the 1990s, computational simulations were applied to predict the stress and strain in DC casting. Drezet and Rappaz developed a three dimensional model in ABAQUS to predict the ingot distortion [3]. The numerical and measured results agreed with each other in terms of the pull-in of the ingots' rolling faces. Since then, more sophisticated finite element models have been built to calculate the stress level in casting ingots [4, 5, 6, 7]. Advanced experimental validation techniques such as neutron diffraction has been applied to validate the predicted stress level [4, 5]. It has become a well-established approach to study stress and strain of an industrial casting ingot through inexpensive numerical models.

Recently, there have been more studies on factors influencing the stress levels in DC cast ingots. In 2013, Jamaly et al. demonstrated through an ABAQUS model that a slower casting speed and a lower mechanical coalescence temperature (accomplished by reducing grain size) resulted in a smaller hot tearing strain [8]. Also, Drezet and Pirling showed that by using a wiper to divert water from the ingot surface far from the mold, the residual stress in an industrial ingot is reduced by a third [5].

However, there are fundamental issues that have not been addressed. Especially for rectangular slabs, practical concerns such as limits to the absolute size of an ingot and how the aspect ratio of the cross section influence the stress level have not been addressed yet and will be discussed in this paper. Also, the effect of the wiper position will be investigated. The current model adopts a more realistic constitutive law including strain hardening from the previous works [8, 9, 10]. Primary cooling with the mold and secondary cooling with chilling water are included in the thermal boundary conditions. The heat transfer coefficient for the primary cooling is assumed as a function of surface temperature by accounting for the air gap [6]. In this way, the difficulty of actually simulating air gap formation is circumvented as compared to the work in [11]. The aim of this paper is to examine the influence of size, aspect ratio, and wiper position in large casting ingots in terms of residual stress.

Model Framework

Finite Element Modeling

The DC casting process of rectangular AA 5182 ingots was modeled in the commercial finite element package ABAQUS - v6.13. One quarter of the ingot was simulated by applying symmetric boundary conditions. Initially, there were 9 layers of elements and each layer has a height of 10 mm. It was held in the mold for 120 s to form a solid shell before withdrawing. To simulate the subsequent continuous inflow of liquid metal, 3 layers of elements were activated on top every 24 seconds to model a casting speed of 75 mm/min and the thermal boundary conditions were moved up 30 mm, as they were fixed to the top of the active domain. The activation of new layers of elements ceased when the ingot reached a height of 300 mm. The pouring temperature of the alloy melt was 637°C. A 0.5 h cooling period was simulated. Hence the total simulation time was 120 s for the initial holding, 144 s for casting, plus 1800 s for cooling. The CPU time required was around 100 h for Intel(R) Xeon(R) CPU E3-1225 V2 @ 3.20 GHz processor.

AA5182 Materials Properties

AA 5182 alloy (4.5 wt.% Mg) has a relatively wide freezing range from 523 °C to 637 °C [12]. The coalescence temperature at which the ingot starts to have a mechanical response is a function of grain size, and it is assumed to be 602 °C based on the range from Jamaly et al.'s work [8]. Below the coalescence temperature, Young's modulus and thermal expansion coefficient (CTE) are temperature dependent, while above they are not significant and

represented in the model by small values. The current model used the Young's modulus in the solid state (below 523 °C) measured by Alankar [10], and assumed a linear decrease to zero between freezing point and coalescence temperature, as shown in Figure 1.

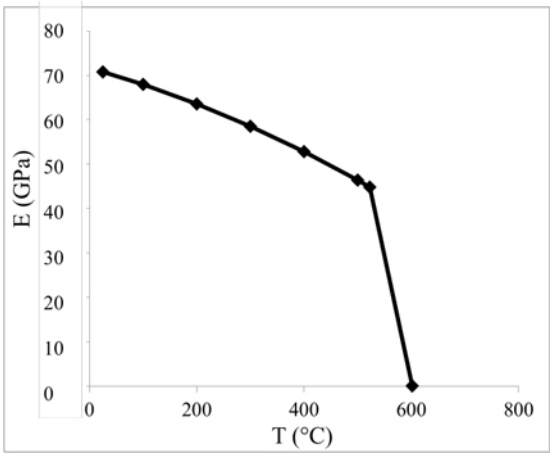

Figure 1. Young's modulus as a function of temperature for AA5182 alloy [10].

The CTE was estimated based on the work by Nix and MacNair [13], as shown in Figure 2.

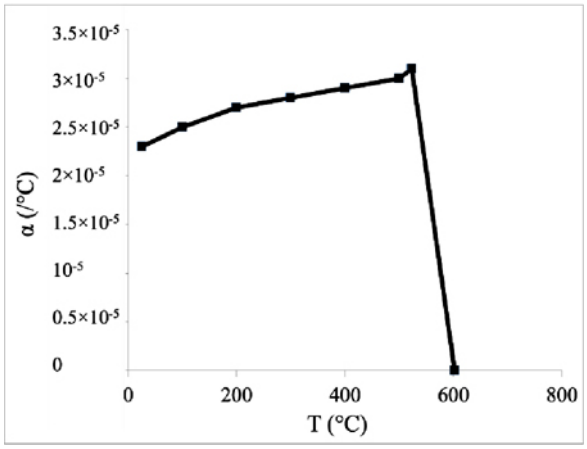

Figure 2. CTE as a function of temperature for AA5182 alloy [13].

The mechanical behavior of AA 5812 is modeled through the use of the modified Ludwik Equation [8, 9, 10],

$$\sigma(T,\varepsilon,\dot{\varepsilon}) = K(T)(\varepsilon_p + \varepsilon_{p_o})^{n(T)}(\dot{\varepsilon}_p + \dot{\varepsilon}_{p_o})^{m(T)} . \quad (1)$$

Here, σ is the stress, and is dependent on temperature (T), strain (ε) and strain rate ($\dot{\varepsilon}$). K is a material constant, ε_p is the plastic strain. $\dot{\varepsilon}_p$ is the strain rate, n is the strain hardening coefficient, and m is stain-rate hardening coefficient. The current model used values for K, n and m below 500 °C measured by Alankar and Wells [10] (Table 1). The mechanical behavior was extrapolated in the semi-solid state, as Drezet and Phillion demonstrated that the constitutive law at solid state dominates the residual stress level [4]. Also, only the strain-hardening effect was taken into account, and the less significant strain rate hardening effect was ignored [6], *i.e.*, the strain rate ($\dot{\varepsilon}_p$) is treated as a constant, $10^{-5}s^{-1}$. The stresses and corresponding plastic strains were implemented through ABAQUS tabular input.

Table 1. Stress-Strain-Temperature Coefficient for AA5182 [10].

Parameter	Temperature Range(°C)	Correlation
K	$25 < T < 331$	$K = -0.3409T + 361.83$
	$331 < T < 500$	$K = -1.1015T + 613.59$
n	$25 < T < 206$	$n = -0.0003T + 0.17$
	$206 < T < 361$	$n = -0.0007T + 0.252$
	$361 < T < 500$	$n = 0$
m	$25 < T < 183$	$m = 0$
	$183 < T < 361$	$m = 0.001T - 0.183$
	$361 < T < 500$	$m = 0.0003T + 0.069$

Thermal Boundary Conditions

The heat transfer of the ingot in contact with the mold (primary cooling) is modeled by implementing the experimental heat transfer coefficient (HTC) correlations as a function of surface temperature by Hao et al. [6], as shown in Figure 3. The computational cost is reduced because the need of adding a simulation domain of air and modeling the air-mold-ingot contact is avoided. When the ingot leaves the mold, the heat extracted from the chilling water (secondary cooling) is simplified and modeled by a constant HTC of 10000 W/m^2/K [2]. Below the wiper, a HTC of 20 W/m^2/K in contact with the air (tertiary cooling) is approximated based on [6]. Finally, the heat extracted from the bottom is modeled by a HTC of 200 W/m^2/K, following Drezet and Pirling [5]. The ambient temperature of the water and mold is assumed to be 20 °C.

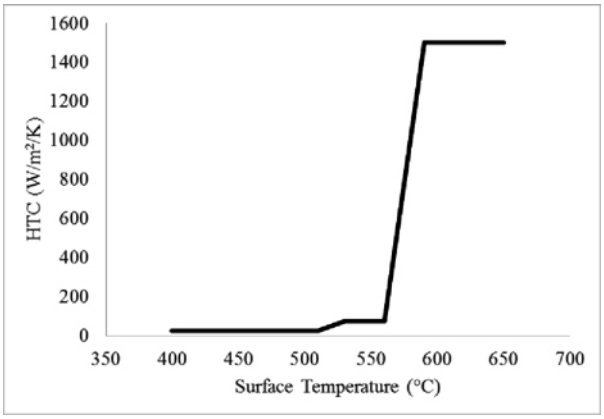

Figure 3. Primary cooling heat transfer coefficient. It decreases with respect to temperature as the air gap forms when the ingot shrinks [10].

Results and Discussions

Comparison between Slab and Round

Two simulations were developed to compare the residual stress level for rectangular and round ingots. The rectangular ingot had a cross-section of 20 × 20 cm, and the round ingot had a radius of 11.3 cm, so the cross-sectional areas were the same. A wiper was placed at 9 cm below the casting mold for both simulations.

Figure 4 shows the temperature fields of the slab and round at t = 264 s. They have very similar sump shape and depth, as indicated by the temperature distribution. The round ingot has a slightly more uniform temperature distribution. Both ingots have similar temperatures at the center (within 5 °C), and the round's lowest temperature point (between mold and wiper) was 50 °C hotter than the similar point on the slab. That is because the slab has a larger side wall area (by 10%) for cooling compared to the round ingot.

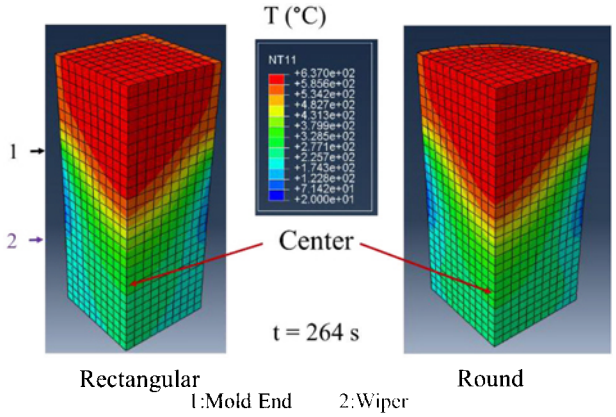

Figure 4. Temperature profiles of slab and log at t = 264 s. Red represents hotter (liquid) region, while blue and green represent colder (solid) region. The coldest points are on the surface between the mold and wiper, below which the temperature rebounds. The two sumps have similar shapes.

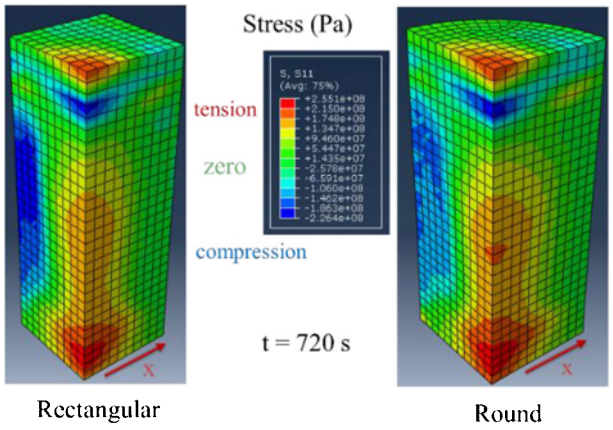

Figure 5. Residual stress levels of slab and round at t = 720 s. Red represents the tensile stress and blue the compressive. Both ingots have tension in the center and compression at the surface.

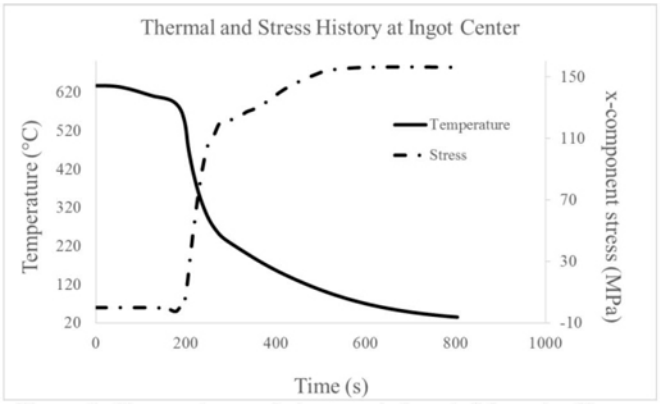

Figure 6. Temperature and stress evolution at slab center (6 cm above bottom). Temperature decreases slowly from the beginning to 200 s, and rapidly from 200 s to 400 s. As a result, tension increases suddenly from 200 s.

The similar sump shapes lead to similar residual stress levels after cooling, as seen by the x-component stress in Figure 5. For both ingots, tension develops in the center at the ingot bottom, while the surfaces are under compression (the "skin-core" effect [4, 14]). The two ingots have very similar peak tension levels at the center, while the round has a slight lower (7%) peak compression value at its surface.

The temperature and stress evolution in the slab center, 6 cm above the bottom, are shown in Figure 6. Tensile stress starts to grow because the contraction in ingot center is restrained by the already solidified outer layer. Also, the tension develops the fastest when the temperature change is most rapid, suggesting that reducing cooling rate will reduce residual stress level.

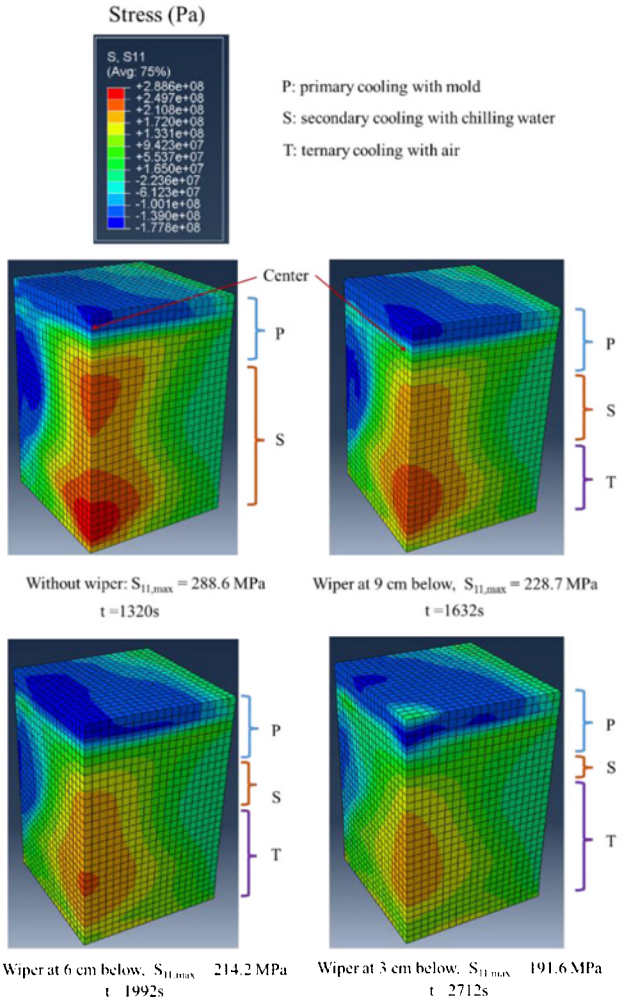

Figure 7. As-cast residual stress levels for rectangular ingots without a wiper, and with wipers placed 9 cm, 6 cm and 3 cm below the mold. Ingots with wipers closer to the mold have lower centerline tensile stress.

Influence of a wiper and wiper position

Figure 7 shows the stress profiles of slabs (40 cm × 40 cm cross-section) with different wiper arrangements: without a wiper, and with a wiper placed at 9 cm, 6 cm, and 3 cm below the mold. They were recorded when the maximum ingot temperature was 10 °C above the ambient. The higher the wiper is placed, the slower the cooling rate is and the longer the solidification and cooling times. By placing a wiper 3 cm below, it needs twice the time compared to the ingot without wiper. The major benefit of a slower cooling rate is less residual stress. As shown in Figure 7, the maximum x-component stress (S_{11}) at the ingot center is reduced by 20% for placing wiper 9 cm below the mold, 26% for 6 cm, and 34% for 3 cm compared to the case without the existence of a wiper. Meanwhile, the volume (represented by red and orange regions in Figure 7) subjected to the high tensile stress (over 200 MPa) decreases together with stress magnitude when the wiper is placed higher.

However, there exists a certain limit of height at which the wiper can be placed, as placing it above that position will result in the remelting of the ingot surface. As shown in Figure 8, the lower half of the ingot becomes very close to semi-solid state (the peak ingot temperature below the wiper is 526 °C, while the solid point is 537 °C) when the wiper is placed 3 cm below the mold. A slight increase in the degree of superheating or casting speed or local segregation would cause incipient melting at the ingot surface at this point. Hence, the height limit for a 40 cm × 40 cm ingot is close to 3 cm below the mold. Another solution to remelting below wiper is to raise the wiper position as solidification progresses, *e.g.*, initially at 9 cm and gradually lift it to 3 cm.

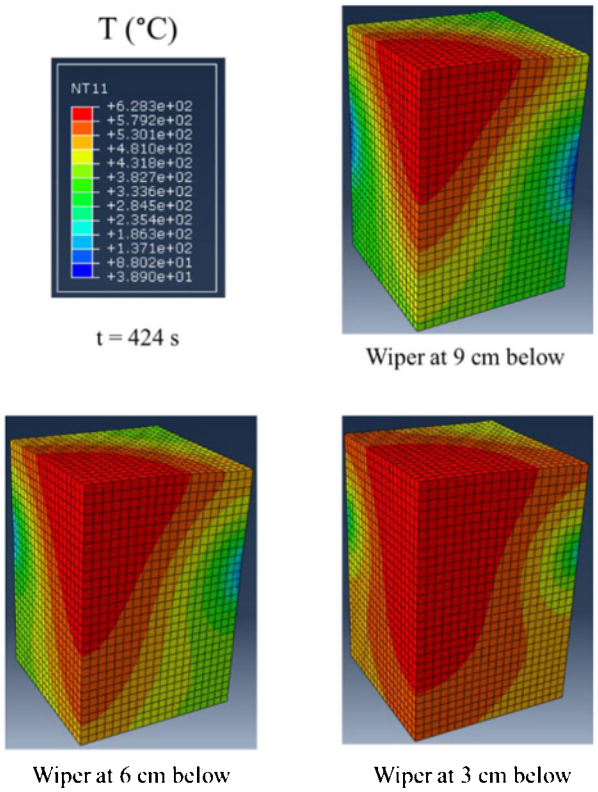

Figure 8. Temperate profiles of ingots with a wiper placed at 9 cm, 6 cm, and 3 cm below the mold. As the wiper is placed higher, the sump became wider. Eventually, the surface is susceptible of being partially remelted when the wiper is placed close to the mold.

Influence of Slab Aspect Ratio

The stress profiles of slabs with aspect ratios ranging from 1 to 3 are shown in Figure 9. The cross sections of the slabs are 20 cm × 20 cm (A = 1), 20 cm × 40 cm (A = 2) and 20 cm × 60 cm (A = 3), and a wiper is placed 9 cm below the mold for all the three ingots. By introducing an aspect ratio larger than one, the tensile stress in the ingot center along the short edge (S_{11}) is reduced (see left column in Figure 9). On the other hand, the tensile stress along the long edge (S_{22}) affects a much larger volume of the ingot with a similar magnitude compared to the one with A = 1 (see right column in Figure 9). Also, the volume (red and orange regions) subjected to high tension (150 MPa) increases with increasing aspect ratio because a larger temperature gradient is established

along the long edge. The results suggest that fabricating an ingot with aspect ratio larger than one would significantly reduce the tension along the short edge, and concentrate tension along the long edge at the same time, which renders the slabs prone to surface cracks along the long edge.

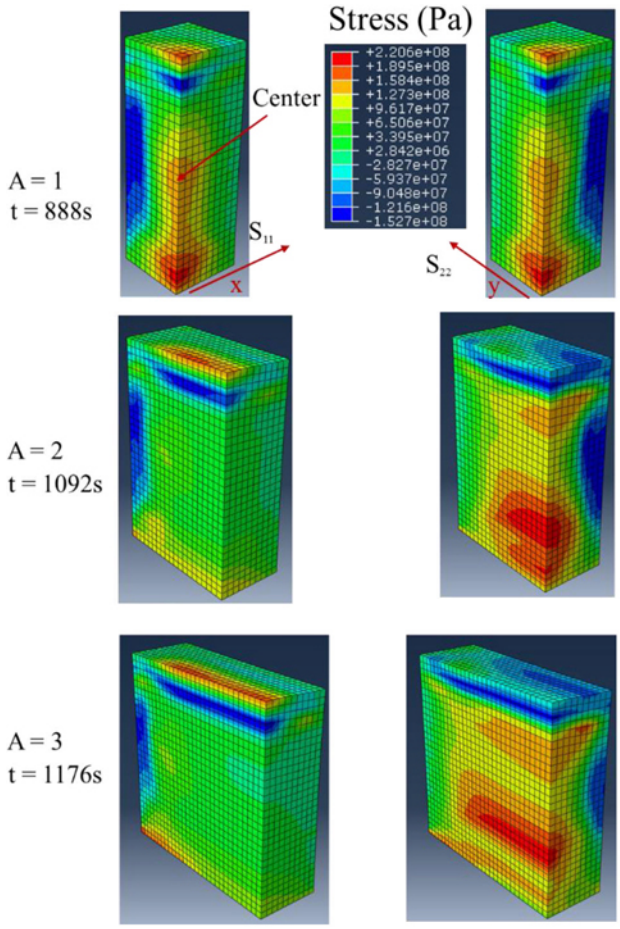

Figure 9. Stress profiles (S_{11} on the left, S_{22} on the right) of ingots with aspect ratios of 1, 2, and 3. The S_{11} component of stress is less tensile at larger aspect ratios, but a larger volume of the ingot is subjected to high tension.

Influence of Absolute Size

Figure 11 shows the residual stress level for slabs with a square cross section but different sizes: 20 cm × 20 cm, 32 cm × 32 cm, and 40 cm × 40 cm. A wiper is placed 9 cm below the mold for all three ingots. The magnitude of the tension at center is insensitive to change in ingot size, but the tension affects a much larger volume fraction as a result of deeper and wider sump in larger casting ingots (See Figure 10). Central regions in larger ingots would stay in semi-solid state for a longer period. Hence, larger ingots are more susceptible to tearing.

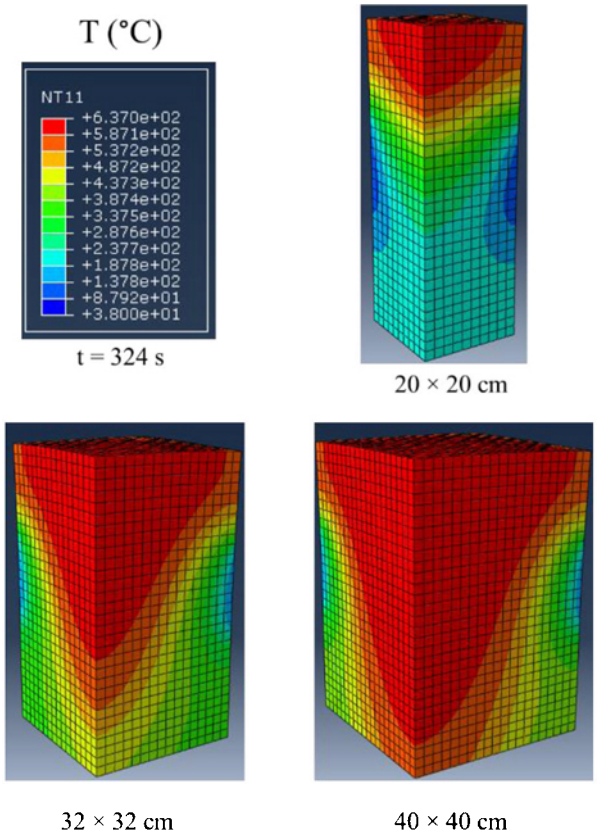

Figure 10. Temperature profiles of ingots with a cross section ranging from. 20 cm × 20 cm, 32 cm × 32 cm, and 40 cm × 40 cm. The temperature difference from center to edge is bigger in larger ingots, where deeper and wider sumps are identified.

Conclusions

In this paper, a coupled thermomechanical model is used to predict the residual stress for DC casting ingots. Primary cooling, secondary cooling, cooling from bottom, and the effect of a wiper are included. Numerical predictions suggest that the addition of a wiper decreases the residual tension in ingot center, and the tension is further reduced by placing the wiper closer to the mold. The model results show that, if the wiper is placed too close to the mold, the surface will partially remelt, leading to surface defects and possible bleed-out. Also, results indicate that larger ingots and slabs with larger aspect ratios have a higher overall tension level due to a larger temperature gradient.

With the simplified thermal boundary conditions and the capability of quantitatively predicting residual stress, the current finite element model has the potential to be applied to optimize fabrication conditions for industrial DC casting. The implementation of applying a moving wiper is proposed, in order to combine the merit of a slower cooling rate and having solid ingot skin, which should be studied further.

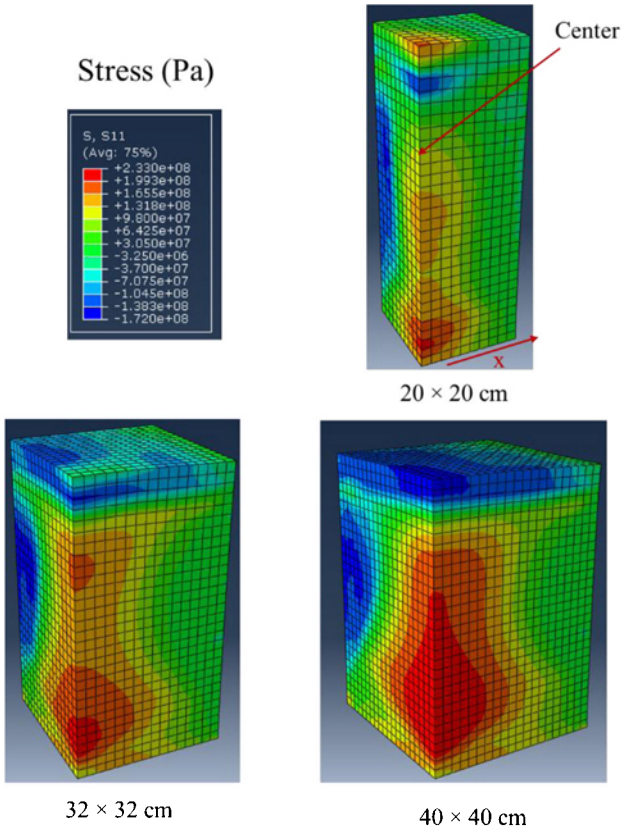

Figure 11. Stress profiles of ingots with cross sections of 20 cm × 20 cm, 32 cm × 32 cm, and 40 cm × 40 cm. Larger ingots have more volume subjected to the high tension in the ingot center.

Acknowledgement

The authors would like to thank the Nanshan Aluminum, Beijing Institute of Aeronautical Materials and Nanshan America for their financial support for this work.

References

[1] D. C. Weckman and P. Niessen, "Mathematical Models of the D.C. Continuous Casting Process," *Can. Metall. Q.*, vol. 23, no. 2, pp. 209–216, Apr. 1984.

[2] D. Weckman and P. Niessen, "A numerical simulation of the DC continuous casting process including nucleate boiling heat transfer," *Metall. Trans. B*, vol. 13, no. December, pp. 593–602, 1982.

[3] J. Drezet and M. Rappaz, "Modeling of ingot distortions during direct chill casting of aluminum alloys," *Metall. Mater. Trans. A*, vol. 27, no. October, 1996.

[4] J. Drezet and A. B. Phillion, "As-Cast Residual Stresses in an Aluminum Alloy AA6063 Billet: Neutron Diffraction Measurements and Finite Element Modeling," *Metall. Mater. Trans. A*, vol. 41, no. 13, pp. 3396–3404, Oct. 2010.

[5] J. Drezet and T. Pirling, "Influence of a wiper on residual stresses in AA7050 rolling plate ingots," *J. Mater. Process. Technol.*, vol. 214, no. 7, pp. 1372–1378, Jul. 2014.

[6] H. Hao, D. M. Maijer, M. A. Wells, S. L. Cockcroft, D. Sediako, and S. Hibbins, "Development and Validation of a Thermal Model of the Direct Chill Casting of AZ31 Magnesium Billets," vol. 35, no. December, 2004.

[7] J. Sengupta, S. L. Cockcroft, D. M. Maijer, and A. Larouche, "Quantification of temperature, stress, and strain fields during the start-up phase of direct chill casting process by using a 3D fully coupled thermal and stress model for AA5182 ingots," *Mater. Sci. Eng. A*, vol. 397, no. 1–2, pp. 157–177, Apr. 2005.

[8] N. Jamaly, A. B. Phillion, and J. Drezet, "Stress–Strain Predictions of Semisolid Al-Mg-Mn Alloys During Direct Chill Casting: Effects of Microstructure and Process Variables," *Metall. Mater. Trans. B*, vol. 44, no. 5, pp. 1287–1295, Jul. 2013.

[9] W. Van Haaften and B. Magnin, "Constitutive behavior of as-cast AA1050, AA3104, and AA5182," *Mater. Trans. A*, vol. 33, no. July, 2002.

[10] A. Alankar and M. A. Wells, "Constitutive behavior of as-cast aluminum alloys AA3104, AA5182 and AA6111 at below solidus temperatures," *Mater. Sci. Eng. A*, vol. 527, no. 29–30, pp. 7812–7820, Nov. 2010.

[11] J. Sengupta, S. Cockcroft, and D. Maijer, "On the development of a three-dimensional transient thermal model to predict ingot cooling behavior during the start-up phase of the direct chill-casting process for an AA5182 aluminum alloy," *Mater. Trans. B*, vol. 35, no. 3, pp. 523–540, 2004.

[12] N. Jamaly and A. Phillion, "Hot Tearing Susceptibility in DC Cast Aluminum Alloys," *TMS Proc.*, vol. 2, no. 1, pp. 259–266, 2012.

[13] F. Nix and D. MacNair, "The thermal expansion of pure metals: copper, gold, aluminum, nickel, and iron," *Phys. Rev.*, vol. 10, no. 1926, pp. 7812–7820, 1941.

[14] F. Heymes, B. Commet, B. Du Bost, P. Lassince, P. Lequeu, and G. M. Raynaud, "Development of new Al alloys for distortion free machined aluminium aircraft components," *ASM Int.*, pp. 249–255, 1997.